



Article

Improved Equivalent Strain Method for Fatigue Life of Automobile Aluminum Alloy

Shanjie Zhi¹, Hejian Liu¹ and Xintian Liu^{2,*}

¹ College of Engineering, Applied Technology College of Soochow University, Suzhou 215000, China; zhishanjie@suda.edu.cn (S.Z.); liuhejian@suda.edu.cn (H.L.)

² School of Mechanical and Automotive Engineering, Shanghai University of Engineering Science, Shanghai 201600, China

* Correspondence: xintianster@sues.edu.cn

Abstract: Automotive parts are usually subjected to random loads with large mean tensile/compressive stresses under working conditions. It is important for automotive parts to have a long fatigue life under mean stress in practical engineering applications. An equivalent strain model is established here to predict fatigue life considering the influence of mean strain and stress under asymmetric cycles. To predict the fatigue life more accurately, the coefficient of surface roughness and temperature correction is introduced in this model. The effectiveness of the improved equivalent strain (IES) model is verified by comparing it with multiple sets of experimental data. The IES is also compared with Smith–Watson–Topper (SWT), Manson–Coffin, and equivalent strain models. The results show that the developed model has a higher prediction accuracy than the other models. An improved fatigue strength exponent is introduced to modify the equivalent strain model, and the effectiveness of the model is verified by experimental data. The IES model demonstrates significantly reduced standard deviations under various strain ratios (−0.06, 0.06, 0.5), with measurements of 0.0936, 0.0721, and 0.0636, respectively. The method provides a certain reference for the life prediction of automotive parts.

Keywords: fatigue life; surface roughness coefficient; temperature correction coefficient; improved equivalent strain model; life prediction



Citation: Zhi, S.; Liu, H.; Liu, X.

Improved Equivalent Strain Method for Fatigue Life of Automobile Aluminum Alloy. *World Electr. Veh. J.* **2024**, *15*, 200. <https://doi.org/10.3390/wevj15050200>

Academic Editor: Joeri Van Mierlo

Received: 1 April 2024

Revised: 1 May 2024

Accepted: 2 May 2024

Published: 6 May 2024



Copyright: © 2024 by the authors. Licensee MDPI, Basel, Switzerland. This article is an open access article distributed under the terms and conditions of the Creative Commons Attribution (CC BY) license (<https://creativecommons.org/licenses/by/4.0/>).

1. Introduction

The fatigue or failure of metal materials is the process of the gradual accumulation of damage, the generation of cracks, and crack propagation until the final failure of metal materials under the action of alternating load [1,2]. Most mechanical structure damage is caused by fatigue [3,4]. Fatigue life prediction has always been a concern within engineering and academic circles [5–7].

Fatigue life prediction is an effective method for preventing major accidents. Symmetrical cyclic loading is commonly used under laboratory conditions but is rarely found in actual engineering applications [8,9]. Most mechanical components usually suffer from an asymmetric fatigue load [10], and the effect of mean stress should be considered to improve models for the prediction of fatigue life. In general, cyclic loading significantly affects the damage accumulation process of components [11]. The influence of mean strain and mean stress on the fatigue behavior of materials is reciprocal. Applying mean strain is equivalent to introducing a pre-strain, which, under certain circumstances, can deplete a portion of the material's effective ductility, thereby reducing its fatigue life. In the most extreme scenario, when the mean strain reaches the material's monotonic fracture ductility, the material exhausts all inherent ductility, resulting in ductile failure. Furthermore, some experimental results indicate that non-elastic pre-strain can significantly decrease the fatigue life of a material under subsequent low-load conditions much more severely than the predicted

reduction in fatigue life directly caused by pre-strain-induced damage. Mean stress also plays a significant role in the initiation of fatigue cracks in engineering components. It is generally believed that tensile mean stress shortens the fatigue life, while compressive mean stress prolongs the fatigue life [7].

When both mean strain and mean stress exist simultaneously, especially in the presence of significant cyclic plastic strain, mean stress plays a primary role in fatigue behavior. During stress-controlled testing, tensile mean stress causes the mean strain to gradually increase along the tensile direction, thereby generating a strain ratcheting effect; whereas in asymmetric strain-controlled testing, plastic strain causes the larger mean stress to gradually decrease or even disappear, leading to the phenomenon of mean stress relaxation. During low cycle fatigue processes, due to the presence of a large amount of plastic strain, the mean stress undergoes a process of generation, disappearance, or change. The phenomenon of a gradual decrease in mean stress with cyclic loading is referred to as mean stress relaxation. Surface treatment methods such as shot peening reinforcement are often adopted in engineering to introduce surface residual compressive stress and improve the fatigue life of materials or components. However, mean stress relaxation affects the initiation and propagation of fatigue cracks by reducing beneficial residual stresses on the surface. The phenomenon of mean stress relaxation is caused by the presence of cyclic plastic strain amplitudes. As the total strain amplitude increases, the plastic strain amplitude also increases. Therefore, with larger strain amplitudes, the rate of mean stress relaxation is higher. In cases of small strain amplitude control, the plastic strain is almost close to zero. Thus, when the strain amplitude is small, mean stress relaxation is not significant. Engineering components are often affected by alternating and mean stress under the normal strain ratio. The mean stress effect has a greater impact on the crack initiation process and fatigue life than the other effects [12]. The function of mean stress and amplitude is usually used to express the effect in the fatigue life. The load amplitude of the endurance limit decreases with mean stress in a special cyclic loading process [13,14]. If the minimum stress is less than the complete reverse constant amplitude fatigue limit and the maximum stress remains unchanged, the error could be corrected by maintaining the maximum and reducing the minimum [15].

The fatigue limit for the material micro-defects is given by the difference in stress concentration behavior. The formula is suitable for the compression mean stress state and introduces the mean stress correction parameter and the fatigue limit effect can be expressed by the dependence of the mean stress [16]. Some mean stress correction methods and fatigue behavior theories have been proposed with the establishment of empirical formulas for different metal materials, such as the Gerber, Morrow, Goodman, SWT, and equivalent strain methods [17,18].

Different materials have different mechanical properties and mean stress effects. Several models have been proposed to estimate the fatigue life considering the effect of mean stress. Lv et al. combined the parameters of the Walker and SWT models to propose a strain life model based on the mean stress sensitivity of the material [19]. Vantadori et al. have calculated the fatigue life of Inconel 718 specimens under uniaxial/biaxial loading by considering the mean stress effect in SWT type [20]. Liu proposed the universal multi-axial fatigue life prediction model by using the mean stress effect of the axial and torsional [21]. Zhu et al. established an energy-based fatigue life prediction model using two mean stress correction factors [22]. The Walker exponent is used to modify the effective strain energy density model [23]. Kluger and Lagoda considered the variability in material properties with non-parallel fatigue characteristics and mean torsional stress, and proposed a combined fatigue life estimation method based on the Kluger stress criterion [24].

Several fatigue life prediction criteria have been developed to calculate cumulative damage based on fracture mechanics, energy, strain, and stress methods [25]. The mean stress effect should be considered in strain-controlled uniaxial and multiaxial fatigue tests. Some scholars put forward several models with the influence of mean stress under uniaxial fatigue loads [26–28]. The mean stress of 316 stainless steel does not need to be corrected

using the load control mode or by changing the component design of the ratchet strain restriction zone [29]. Wang et al. have studied the effect of the fatigue strength exponent on fatigue life [30]. Liang collected crack closure behavior and effective crack growth rate data for various steels, showing that the effective crack growth rate is independent of the steel's hardness and R-ratio [31].

Aluminum alloys are widely utilized in automotive manufacturing. Lukács established fatigue design curves for two aluminum alloys (5754-H22 and 6082-T6) and their corresponding welded joints produced using the Friction Stir Welding (FSW) technique [32]. Fu investigated the low-cycle fatigue (LCF) life and failure mechanisms of 7075-T6 high-strength aluminum alloys under MTS 809 conditions, as well as their cycling stress responses and cyclic stress–strain relationships under different strain amplitudes [33].

The influence of mean stress on fatigue life has been extensively studied and discussed by numerous researchers [15]. However, the effect of the fatigue strength exponent has received relatively less attention. The fatigue strength exponent is modified by introducing surface roughness and the temperature correction coefficient, and is verified using several groups of test data. The IES model is proposed based on the effects of mean stress and the fatigue strength exponent. The main content is as follows. In Section 2.1, several common mean stress correction methods used in strain-life analysis are introduced. In Section 2.2, an equivalent strain model based on the modified fatigue strength exponent is proposed. In Section 3, the improved model (IES) is validated with experimental data and compared with the Manson–Coffin, SWT, and ES methods to evaluate the effectiveness and accuracy of the proposed model. The conclusion section emphasizes the importance of considering both mean stress and the fatigue strength exponent in fatigue life prediction and provides insights into potential future research directions. Through this comprehensive investigation, we aim to enhance our understanding of the complex relationship between mean stress, fatigue strength exponent, and fatigue life. By incorporating these factors, we can improve the accuracy of fatigue life prediction models and contribute to the development of more reliable and efficient engineering designs.

2. Materials and Methods

2.1. Strain-Based Life Prediction Methods

Fatigue life can be accurately predicted by establishing an accurate model with good prediction performance [34–36]. In the case of high cycle fatigue, the elastic strain leads to failure, and the plastic strain can be ignored. The S-N curve expression can be given based on the law of fatigue characteristics of metal materials. There was a linear relationship between the stress amplitude and the number of fatigue cycles in the double logarithm coordinate, and the expression can be defined as follows:

$$\sigma_a = \sigma'_f (2N_f)^b \quad (1)$$

where σ_a is the stress amplitude, N_f is the number of cycles to failure, σ'_f is the fatigue strength coefficient, and b is the fatigue strength exponent.

If the cyclic stress amplitude is higher, the fatigue life is relatively low. The load amplitude of the material is higher than the yield limit, the plastic deformation of the structure will occur under low cycle fatigue, and the material will undergo cyclic hardening or softening under high amplitude alternating stress loading. The strain can be obtained in a low cycle fatigue test. The cyclic nature of the loading leads to a gradual accumulation of strain that can ultimately lead to failure. It is essential to monitor and analyze the strain development to predict the material's fatigue life accurately. Furthermore, in the presence of high cyclic stress amplitudes, the material may undergo changes in its microstructure, leading to variations in its mechanical properties over time. This phenomenon can influence the material's fatigue behavior, impacting its durability and longevity under cyclic loading conditions.

Based on the effect of temperature of ductile materials, the plastic strain amplitude can be used to describe the life in the low cycle fatigue [37]. The linear relationship between plastic strain amplitude and fatigue failure life can be expressed in a logarithmic coordinate:

$$\varepsilon_{pa} = \varepsilon'_f (2N_f)^c \quad (2)$$

where ε_{pa} is the plastic strain amplitude, c is the fatigue ductility exponent, and ε'_f is the fatigue ductility coefficient.

According to Hooke's law, the elastic strain under high cycle fatigue conditions can be expressed as follows:

$$\varepsilon_{ea} = \frac{\sigma_a}{E} = \frac{\sigma'_f}{E} (2N_f)^b \quad (3)$$

The total strain amplitude is the sum of the plastic ε_{pa} and elastic ε_{ea} , as follows:

$$\varepsilon_a = \varepsilon_{ea} + \varepsilon_{pa} \quad (4)$$

The Manson–Coffin prediction model can be used to obtain strain life fatigue as follows:

$$\varepsilon_a = \frac{\sigma'_f}{E} (2N_f)^b + \varepsilon'_f (2N_f)^c \quad (5)$$

where E is the elastic modulus.

The strain can be obtained using measurement methods. The local strain of the component can be obtained with the Manson–Coffin formula. The ε - N curve for low cycle fatigue has been widely used in practical engineering, and the influence of mean stress σ_m or strain ε_m should be considered and discussed in an asymmetric strain cycle.

The effect of mean stress on the longer life region is greater than the shorter one [38]. The Morrow model can be expressed based on the elastic strain as follows:

$$\varepsilon_a = \frac{\sigma'_f - \sigma_m}{E} (2N_f)^b + \varepsilon'_f (2N_f)^c \quad (6)$$

The Manson–Coffin model can be given by modifying SWT as follows:

$$\sigma_{\max} \varepsilon_a = \frac{(\sigma'_f)^2}{E} (2N_f)^{2b} + \varepsilon'_f \sigma'_f (2N_f)^{b+c} \quad (7)$$

This method combined with the local strain method is widely applied in practical engineering. According to Equation (7), the model considers the influence of mean stress on fatigue life. The results can be obtained by this method, and can then be compared with the experimental results for materials such as grey cast iron, carbon steel, low alloy steel, and so on.

The Manson–Coffin equation is the most classical method for describing the relationship between strain amplitude and fatigue life. This equation divides total strain into elastic strain and plastic strain, which are calculated using Hooke's law and plastic deformation theory, respectively. The Manson–Coffin formula reflects the influence of elastic and plastic strains on fatigue life. When the strain amplitude is large, plastic strain dominates the life. In contrast, when the strain is small, the material deformation remains in the elastic stage, and elastic strain plays a major role. The transition period corresponding to the intersection of these two components is the point where elastic and plastic contributions are equal. The strain–life curve obtained from the Manson–Coffin formula can be fitted with a large amount of experimental data; thus, the more levels of strain tested, the more precise the formula parameters obtained. Both plastic and elastic strain amplitudes in the Manson–Coffin equation are obtained at half-life in low cycle fatigue. This is because the material exhibits cyclic hardening or softening during the testing process. However, this

phenomenon stabilizes after several cycles, and we consider half-life as the steady state of the cycling process. Therefore, plastic strain and elastic strain corresponding to half-life are fitted.

The equivalent strain method, initially introduced in the United States and extensively utilized in aircraft design, offers a systematic approach to predicting fatigue life by accounting for the effects of both mean strain and stress on material fatigue. An advantage of this method is its effectiveness in forecasting fatigue life under asymmetric loading conditions, which will be particularly beneficial in real-world scenarios with complex cyclic loading patterns. Employing the Manson–Coffin model, key parameters like the ductility coefficient and fatigue strength coefficient inform fatigue life predictions by considering ductility and fatigue strength exponents. While the Manson–Coffin model uses strain amplitude to measure cyclic loading, the equivalent strain method applies an equivalent strain that integrates loading magnitude and cyclical nature for a more comprehensive assessment of fatigue behavior in intricate loading scenarios. By incorporating the equivalent strain, the model enhances accuracy and applicability in fatigue life predictions under realistic conditions. The Manson–Coffin model can be used to obtain the parameters, such as ductility coefficient, fatigue strength coefficient, ductility exponent, and fatigue strength exponent. The strain amplitude ε_a is used in Manson–Coffin, and the equivalent strain $(\varepsilon_a)_{eq}$ is applied.

The strain value ε_a is obtained by the effects of mean stress σ_m , mean strain ε_m , strain amplitude ε_a , and stress amplitude σ_a . The formula can be given as follows:

$$\begin{cases} (\varepsilon_a)_{eq} = \frac{\sigma'_f}{E} (2N_f)^b + \varepsilon'_f (2N_f)^c \\ (\varepsilon_a)_{eq} = \varepsilon_a + A \left(\frac{2\sigma_m \sigma_a}{|\sigma_m| + \sigma_a} \right) \frac{1}{E} + B \left(\frac{2\varepsilon_m \varepsilon_a}{|\varepsilon_m| + \varepsilon_a} \right) \end{cases} \quad (8)$$

where A is the mean stress coefficient, and B is the mean strain coefficient.

2.2. Proposed Model

Fatigue strength exponent b is affected by surface roughness, and is related to the fatigue limit life N_e [39]. In practical engineering, many uncertain factors will affect the fatigue strength of the structure, such as working load, geometry, material properties, temperature, etc. [40]. Surface roughness refers to the irregularities present on the surface of a material. These irregularities can act as stress concentrators, leading to localized stress concentrations that can accelerate crack initiation and propagation, thereby reducing the fatigue life of the material. Temperature correction accounts for the effect of temperature on material properties and fatigue behavior. Changes in temperature can alter material properties such as yield strength, ductility, and fatigue resistance. Higher temperatures can promote faster crack growth rates and accelerate fatigue failure. Fatigue strength exponent b can be modified with the coefficients for surface roughness k_r and temperature correction k_d . Modified fatigue strength exponent b' can be rewritten as follows:

$$b' = b + \frac{\log(k_d k_r)}{\log(2N_e)} \quad (9)$$

The fatigue limits of different materials are shown in Table 1 [41]:

Table 1. Fatigue limit life of materials.

The Materials	N_e
steel and cast iron	10^6
magnesium alloy	10^8
aluminum alloy	5×10^8

According to the working temperature T_F [42], if $70 \leq T_F \leq 1000F$, the correction coefficient k_d can be obtained as follows:

$$k_d = 0.975 + 0.432(10^{-3})T_F - 0.115(10^{-5})T_F^2 + 0.104(10^{-8})T_F^3 - 0.595(10^{-12})T_F^4 \quad (10)$$

The surface roughness coefficient k_r can be calculated as follows [30]:

$$k_r = 1 - a \cdot \lg(4R_a) \cdot \lg\left(\frac{2\sigma_b}{R_{m,N,\min}}\right) \quad (11)$$

where a is a constant, R_a is the surface roughness, σ_b is tensile strength, $R_{m,N,\min}$ is the minimum tensile strength.

The values of a and $R_{m,N,\min}$ for different materials are shown in Table 2 [41]:

Table 2. Constant and minimum tensile strength of different materials.

The Materials	a	$R_{m,N,\min}$ (MPa)
cast aluminum alloy	0.20	133
forging aluminum alloy	0.22	133
steel	0.22	400

If the modified fatigue strength exponent b' is introduced into the equivalent strain (ES) method, the numerical model for improved equivalent strain (IES) method can be given as follows:

$$\begin{cases} (\varepsilon_a)_{eq} = \frac{\sigma'_f}{E} (2N_f)^{b'} + \varepsilon'_f (2N_f)^c \\ (\varepsilon_a)_{eq} = \varepsilon_a + A \left(\frac{2\sigma_m\sigma_a}{|\sigma_m| + \sigma_a} \right) \frac{1}{E} + B \left(\frac{2\varepsilon_m\varepsilon_a}{|\varepsilon_m| + \varepsilon_a} \right) \end{cases} \quad (12)$$

3. Results and Discussion

Reducing the overall mass of the car is beneficial for improving energy consumption and environmental pollution. The body accounts for about 30% to 40% of the weight of the whole vehicle, and reducing the body mass can make the car more lightweight. The 7075 aluminum alloy has some characteristics that allow it to perform better than steel in the collision process, such as a low density, high specific strength and specific stiffness, and a large energy absorption capacity. In Table 3, we present a comparison of static performance parameters between the 7075 aluminum alloy and steel. It is helpful to increase the lightweight effect by using a 7075 aluminum alloy in the car body. The model is validated by the experimental data for 7075 aluminum alloy under different strain ratios [42]. The performance parameters of the aluminum alloy are given in Table 4, such as the elastic modulus E , yield strength $\sigma_{0.2}$, tensile strength σ_b , breaking strength K , elongation δ , and section shrinkage φ . The values of the parameters are shown in Table 5, such as the fatigue strength exponent b , fatigue ductility exponent c , mean stress coefficient A , and mean strain coefficient B . The geometry and dimensions of aluminum alloy specimens are shown in Figure 1.

Table 3. Comparison of static performance parameters between 7075 aluminum alloy and steel.

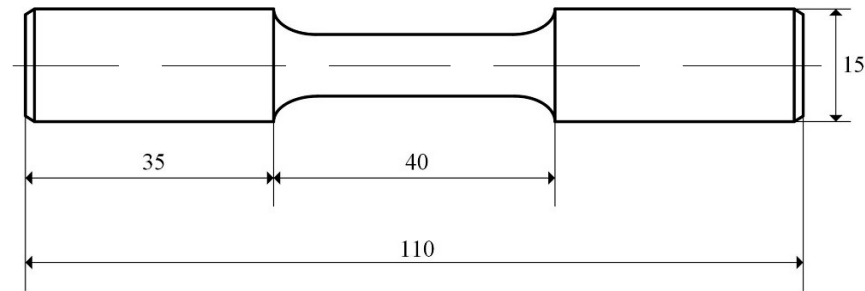
Property	7075 Aluminum Alloy	Steel
Density (kg/m ³)	2810	7850
Elastic Modulus (GPa)	73.48	200–210 (depending on steel type and heat treatment)
Yield Strength (MPa)	439.95	210–1100 (depending on steel type and heat treatment)
Tensile Strength (MPa)	508.12	400–1200 (depending on steel type and heat treatment)

Table 4. Static performance parameters of aluminum alloy.

E (GPa)	$\sigma_{0.2}$ (MPa)	σ_b (MPa)	K (MPa)	δ (%)	φ (%)
73.48	439.95	508.12	591.28	16.33	27.99

Table 5. The values of parameters.

b	c	A	B
-0.07466	-0.53014	0.65289	0.01805

**Figure 1.** The geometry and dimensions of aluminum alloy specimens.

According to Tables 4 and 5, the numerical model for the aluminum alloy can be given as follows:

$$\begin{cases} (\varepsilon_a)_{eq} = 0.00964(2N_f)^{-0.07466 + \frac{\log(k_d k_r)}{\log(2N_f)}} + 0.15015(2N_f)^{-0.53014} \\ (\varepsilon_a)_{eq} = \varepsilon_a + 0.65289 \left(\frac{2\sigma_m \sigma_a}{|\sigma_m| + \sigma_a} \right) \frac{1}{E} - 0.01805 \left(\frac{2\varepsilon_m \varepsilon_a}{|\varepsilon_m| + \varepsilon_a} \right) \end{cases} \quad (13)$$

The low cycle fatigue tests were performed using an MTS-810 electro-hydraulic servo fatigue testing machine, following the guidelines outlined in GB/T 15248-2008 ([43]) titled “The test method for axial loading constant-amplitude low cycle fatigue of metallic materials” The tests were conducted under strain control conditions with a triangular waveform for loading [42]. A 12 mm axial extensometer is attached to the specimen to apply a triangular wave loading.

When selecting strain ratios and strain amplitudes, we carefully considered the specific conditions relevant to automotive components. These components are predominantly subjected to asymmetric cycles in real-world applications. In the symmetrical cycle, the mean strain and stress are both small, and the results of several prediction methods are similar. Therefore, we made the decision not to utilize symmetric cycle data with $R = -1$, as they do not accurately reflect the typical loading conditions experienced by automotive parts. Additionally, smaller strain amplitudes were also not included in our analysis. This decision was based on the observation that the resulting damage at these levels was too minimal to yield meaningful insights into the fatigue behavior of the materials under consideration. Three strain ratios ($R = -0.06$, $R = 0.06$, $R = 0.5$) were chosen for the experiments. Low cycle fatigue tests were conducted at each strain ratio with five different strain amplitudes: 0.6%, 0.8%, 1.0%, 1.5%, and 2.0%. The aluminum alloy specimens were tested for low cycle fatigue at different strain ratios. The working temperature was 25 °C and the surface roughness was $R_a = 0.8 \mu\text{m}$.

The N_f values of four models are shown under strain ratio and amplitude in Tables 6–8.

Table 6. Comparison of the results for four models N_f ($R = -0.06$).

ϵ_a	Test Results	Manson–Coffin	SWT	ES	IES
0.6%	2507	5144.57	4172.68	3796.01	3357.68
0.8%	865.67	1113.93	1234.89	1014.40	946.49
1.0%	449.75	444.11	536.66	423.97	405.36
1.5%	152.25	115.57	146.75	111.47	109.12
2.0%	56.5	52.07	66.04	50.21	49.56

Table 7. Comparison of the results for four models N_f ($R = 0.06$).

ϵ_a	Test Results	Manson–Coffin	SWT	ES	IES
0.6%	2319	5134.43	4023.70	3519.78	3125.96
0.8%	828	1122.57	1219.00	999.37	933.03
1.0%	414	449.99	531.44	419.51	401.21
1.5%	127.5	116.92	146.94	111.15	108.81
2.0%	45.2	52.55	64.80	50.10	49.46

Table 8. Comparison of the results for four models N_f ($R = 0.5$).

ϵ_a	Test Result	Manson–Coffin	SWT	ES	IES
0.6%	2160.67	5501.76	3773.16	3086.30	2760.54
0.8%	810	1201.55	1259.64	969.99	906.86
1.0%	429.33	481.61	562.80	424.58	406.02
1.5%	130	126.81	160.48	117.57	115.01
2.0%	47	58.02	74.90	54.13	53.40

It is easy to identify the errors between the calculated results of several models and the real results, as shown in Figures 2–4.

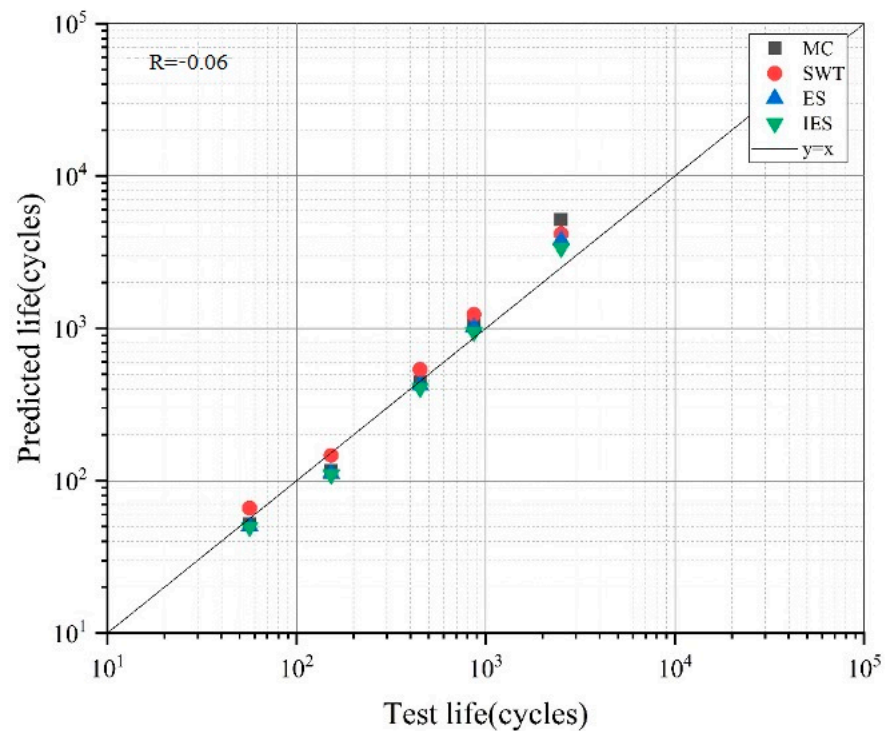


Figure 2. Comparison of the results of the four models ($R = -0.06$).

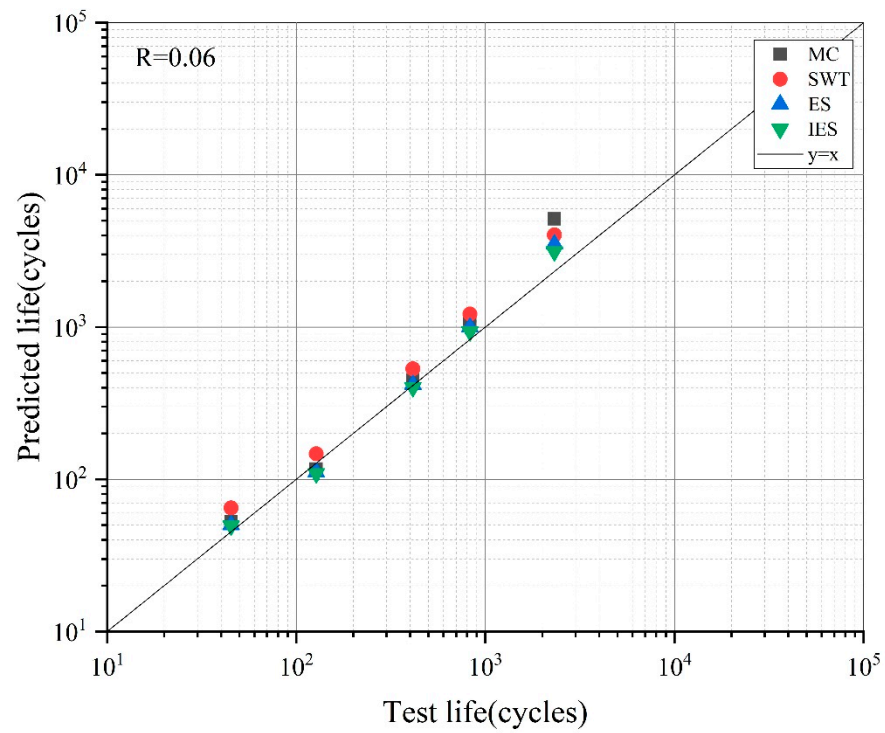


Figure 3. Comparison of the results of the four models (R = 0.06).

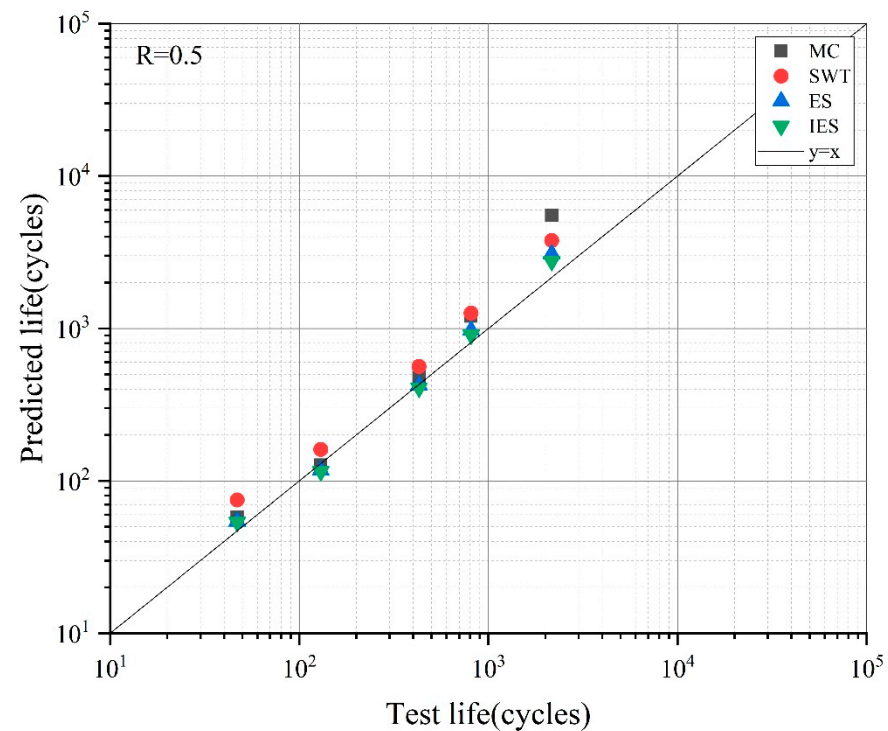


Figure 4. Comparison of the results of the four models (R = 0.5).

To visually compare the errors between the calculated results of several models and the real results, the data were plotted as shown in Figures 2–4. In the context of the illustration, the horizontal axis serves as a representation of the test life, indicating the actual lifespan or endurance of a particular component under evaluation. On the other hand, the vertical axis depicts the predicted life, reflecting the estimated or calculated durability expected based on analytical models or simulations. By comparing the predicted life against the test

life and examining the alignment of data points with the ideal $y = x$ line, researchers can assess the accuracy and reliability of their predictive models in forecasting the performance and longevity of the tested materials or structures.

The closer the predicted lifespan is to the test life, the closer it is to the line $y = x$ in the figure, indicating a smaller margin of error. This observation suggests that the accuracy of the predictive models improves as the calculated lifespan approaches the actual test life. The proximity to the line $y = x$ signifies a higher degree of agreement between the modeled predictions and the real-world outcomes, indicating a reduced discrepancy in and a greater reliability of the predictions.

According to Figure 4, the abscissa value is equal to the ordinate, which means that the test result is equal to the predicted.

Under asymmetric cyclic loading, the error in MC is the largest because the influence of mean strain and stress is neglected, and it is larger than the measured life. The error in the SWT model considering the mean stress correction is also larger than the measured life. The error in the equivalent strain model is lower than that in the MC and SWT models based on the mean stress and strain correction. It can be seen from the figure that the results of the IES model are similar to those of ES for the strain amplitude (1.0%, 1.5% and 2.0%). And the results of IES model are better than those of the ES for the strain amplitude (0.6% and 0.8%).

To assess the accuracy of fatigue life predictions from various models, the predicted life deviation is utilized to measure the alignment between the logarithmic predicted life and the logarithmic experimental life, as demonstrated in Equation (12). Subsequently, the calculation of a standard deviation serves as a metric for evaluating the performance of the life prediction models, as illustrated in Equation (13). A smaller standard deviation indicates a more precise estimation of the predicted life. The standard deviations of fatigue life predictions from the three models are presented in Figure 5. By the deviation between the logarithmic predicted life and the test [44], the errors of fatigue life for different models can be quantified as follows:

$$e = \log_{10}(N_f) - \log_{10}(N_t) \quad (14)$$

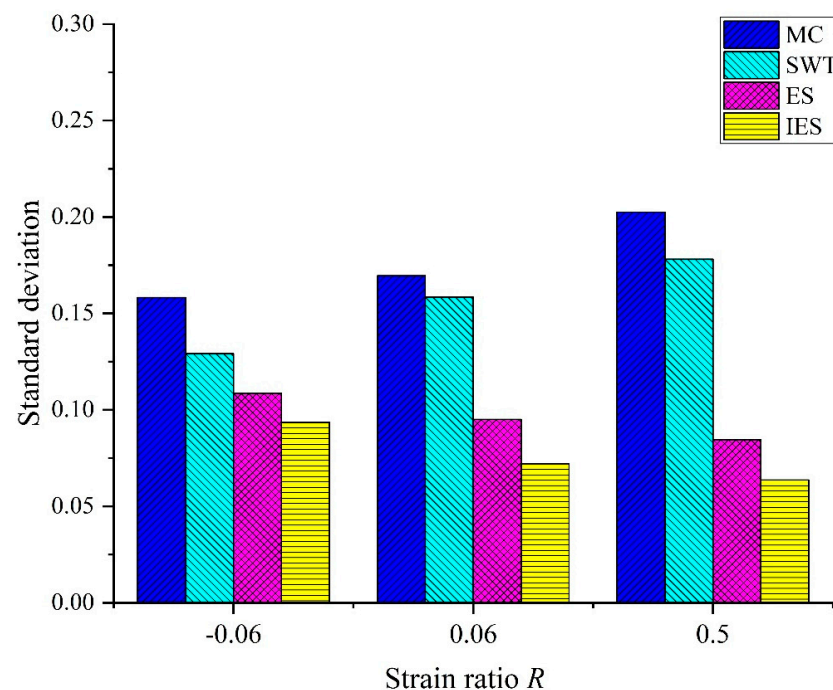


Figure 5. Standard deviation of fatigue life prediction.

The metric of the life prediction model can be expressed by the calculated standard deviation as follows:

$$S_e = \sqrt{\frac{\sum_{i=1}^n e_i^2}{n}} \quad (15)$$

where N_f is the predicted life, N_t is the experimental life, e is the prediction errors in fatigue life, S_e is standard deviation, n is the amount of data.

The smaller the standard deviation, the more the life prediction will be accurate. The standard deviations of four models for fatigue life prediction are shown in Table 9 and Figure 5.

Table 9. Standard deviation of four models for fatigue life prediction.

R	Manson–Coffin	SWT	ES	IES
−0.06	0.1582	0.1292	0.1085	0.0936
0.06	0.1695	0.1584	0.0950	0.0721
0.5	0.2025	0.1781	0.0846	0.0636

As shown in Figure 5, the standard deviations of the MC and SWT models range from 0.12 to 0.21 across various strain ratios, while those of the ES and IES models are consistently below 0.12. Specifically, the standard deviations of the IES model under different strain ratios are notably smaller at 0.0936, 0.0721, and 0.0636, respectively, demonstrating significant improvements compared to the other three models. Notably, the results obtained from the IES model exhibit a closer proximity to the experimental test data when compared to the SWT, MC, and ES models. This enhanced performance can be attributed to the incorporation of an improved fatigue strength exponent in the IES model, resulting in smaller deviations in predicted fatigue life and an overall improved accuracy. In summary, the IES model demonstrates suitability for predicting low cycle fatigue life with greater precision and reduced deviation from the experimental results.

4. Conclusions

In this research paper, the IES model has been utilized to predict fatigue life by enhancing the fatigue strength exponent. The accuracy of the model has been validated using data from three distinct groups of aluminum alloys subjected to varying strain ratios, and comparisons have been made with three other models (MC, SWT, ES). Under asymmetric cycles, the predictions from the IES model closely match the experimental values.

Both the ES and IES models have been scrutinized based on limited data. Going forward, it is recommended that the IES model incorporating mean stress and strain is further evaluated with a broader range of experimental datasets.

There is currently a growing academic discourse surrounding the influence of mean stress on fatigue life, with researchers exploring the impact of the fatigue strength exponent. Modifications to the fatigue strength exponent have led to improvements in the ES model, resulting in enhanced prediction accuracy compared to the original model. Notably, the standard deviations of the IES model under various strain ratios (−0.06, 0.06, 0.5) are significantly smaller, measuring 0.0936, 0.0721, and 0.0636, &ely. Employing the IES model for forecasting the lifespan of automotive components offers greater accuracy and potential cost savings in production.

Future research directions could explore the applicability of the IES model across different materials and operating conditions. Parameters from various materials were input into the IES model to obtain predicted outcomes, which were then compared with experimental data. Further optimization of the parameter determination methods could facilitate the wider application of the IES model in engineering practices, enhancing predictive accuracy and efficiency, and providing a more dependable tool and methodology for material design and component life assessment.

Author Contributions: Conceptualization, S.Z. and X.L.; Methodology, Data curation, Writing—original draft, S.Z.; Writing—review & editing, Data curation, H.L.; Supervision, X.L. All authors have read and agreed to the published version of the manuscript.

Funding: This research received no external funding.

Data Availability Statement: The data that support the findings of this study are available from the corresponding author upon reasonable request.

Conflicts of Interest: The authors declared no potential conflicts of interest with respect to the research, authorship, and/or publication of this article.

Nomenclature

σ_a	stress amplitude
N_f	number of cycles to failure
σ'_f	fatigue strength coefficient
b	fatigue strength exponent
ε_{pa}	plastic strain amplitude
c	fatigue ductility exponent
ε'_f	fatigue ductility coefficient
ε_{ea}	elastic strain amplitude
ε_a	total strain amplitude
E	elastic modulus
σ_m	mean stress
ε_m	mean strain
$(\varepsilon_a)_{eq}$	equivalent strain
A	mean stress coefficient
B	mean strain coefficient
k_r	coefficients for surface roughness
k_d	coefficients for temperature correction
N_e	fatigue limit life
b'	modified fatigue strength exponent
T_F	working temperature
a	constant
R_a	surface roughness
σ_b	tensile strength
$R_{m,N,\min}$	minimum tensile strength
$\sigma_{0.2}$	yield strength
σ_b	tensile strength
K	breaking strength
δ	elongation
φ	section shrinkage
N_t	experimental life
e	prediction errors of fatigue life
S_e	standard deviation
n	amount of data

References

1. Ning, X.; Zheng, S.L.; Xie, W.L. Design principle of active load spectrum for shafting components in wheel hub reducer of electric vehicle. *Proc. Inst. Mech. Eng. Part D J. Automob. Eng.* **2019**, *233*, 2546–2558. [[CrossRef](#)]
2. Santecchia, E.; Hamouda, A.M.S.; Musharavati, F.; Zalnezhad, E.; Cabibbo, M.; El Mehtedi, M.; Spigarelli, S. A Review on Fatigue Life Prediction Methods for Metals. *Adv. Mater. Sci. Eng.* **2016**, *2016*, 9573524. [[CrossRef](#)]
3. Romano, S.; Brückner-Foit, A.; Brandão, A.; Gumpinger, J.; Ghidini, T.; Beretta, S. Fatigue properties of AlSi10Mg obtained by additive manufacturing: Defect-based modelling and prediction of fatigue strength. *Eng. Fract. Mech.* **2018**, *187*, 165–189. [[CrossRef](#)]
4. Ai, Y.; Zhu, S.P.; Liao, D.; Correia, J.A.F.O.; Souto, C.; De Jesus, A.M.P.; Keshtegar, B. Probabilistic modeling of fatigue life distribution and size effect of components with random defects. *Int. J. Fatigue* **2019**, *126*, 165–173. [[CrossRef](#)]
5. Manouchehry, N.R.; Abdullah, S.; Salvinder, S.K.S. Reliability-based fatigue life of vehicle spring under random loading. *Int. J. Struct. Integr.* **2019**, *10*, 737–748. [[CrossRef](#)]

6. Taddesse, A.T.; Zhu, S.P.; Liao, D.; Keshtegar, B. Cyclic plastic zone-based notch analysis and damage evolution model for fatigue life prediction of metals. *Mater. Des.* **2020**, *191*, 108639. [[CrossRef](#)]
7. Su, H.; Wang, J.; Du, J. Fatigue behavior of uncorroded butt welded joints made of bridge weathering steel. *Structures* **2020**, *24*, 377–385. [[CrossRef](#)]
8. Gao, J.X.; Yuan, Y.P.; Xu, R.X. A framework for fatigue life prediction of materials under the multi-level cyclic loading. *Eng. Fail. Anal.* **2021**, *127*, 105496. [[CrossRef](#)]
9. Niesłony, A.; Böhm, M. Mean stress effect correction using constant stress ratio S-N curves. *Int. J. Fatigue* **2013**, *52*, 49–56. [[CrossRef](#)]
10. Zhang, J.; Xiao, Q.; Shi, X.; Fei, B. Effect of mean shear stress on torsion fatigue failure behavior of 2A12-T4 aluminum alloy. *Int. J. Fatigue* **2014**, *67*, 173–182. [[CrossRef](#)]
11. Dowling, N.; Calhoun, C.; Arcari, A. Mean stress effects in stress-life fatigue and the Walker equation. *Fatigue Fract. Eng. Mater. Struct.* **2009**, *32*, 163–179. [[CrossRef](#)]
12. Zhang, J.S. *High Temperature Deformation and Fracture of Materials*; Woodhead Publishing: Sawston, UK, 2010.
13. Klubberg, F.; Klopfer, I.; Broeckmann, C.; Berchtold, R.; Beiss, P. Fatigue testing of materials and components under mean load conditions. *An. Mecánica Fract.* **2011**, *1*, 419–424.
14. Liu, X.T.; Liu, J.Z.; Wang, H.J. Prediction and evaluation of fatigue life considering material parameters distribution characteristic. *Int. J. Struct. Integr.* **2022**, *13*, 309–326. [[CrossRef](#)]
15. da Silva, D.G.; Lockwood, J.; Liang, W.; Topper, T. Mean stress effect in stress-life for hard steels. *Int. J. Fatigue* **2021**, *146*, 106101. [[CrossRef](#)]
16. Cai, X.J.; Li, X.Z.; Xu, J.Q. Fatigue limit and life evaluation formulae for compressive mean stress states. *Mater. Sci. Technol.* **2018**, *34*, 2166–2173. [[CrossRef](#)]
17. Zhu, S.P.; Huang, H.Z.; He, L.P.; Liu, Y.; Wang, Z. A generalized energy-based fatigue-creep damage parameter for life prediction of turbine disk alloys. *Eng. Fract. Mech.* **2012**, *90*, 89–100. [[CrossRef](#)]
18. Ning, X.; Zheng, S.; Wang, Y.; Feng, J. Lightweight design of gears in the wheel-side reducer based on Shanghai road driving cycle. *Proc. Inst. Mech. Eng. Part D J. Automob. Eng.* **2019**, *233*, 1586–1600. [[CrossRef](#)]
19. Lv, Z.; Huang, H.Z.; Wang, H.K.; Gao, H.; Zuo, F.J. Determining the Walker exponent and developing a modified Smith-Watson-Topper parameter model. *J. Mech. Sci. Technol.* **2016**, *30*, 1129–1137. [[CrossRef](#)]
20. Vantadori, S.; Carpinteri, A.; Luciano, R.; Ronchei, C.; Scorza, D.; Zanichelli, A. Mean stress effect on fatigue life estimation for Inconel 718 alloy. *Int. J. Fatigue* **2020**, *133*, 105391. [[CrossRef](#)]
21. Liu, B.W.; Yan, X.Q. A new model of multiaxial fatigue life prediction with the influence of different mean stresses. *Int. J. Damage Mech.* **2019**, *28*, 1323–1343. [[CrossRef](#)]
22. Zhu, S.P.; Lei, Q.; Huang, H.Z.; Yang, Y.J.; Peng, W. Mean stress effect correction in strain energy-based fatigue life prediction of metals. *Int. J. Damage Mech.* **2017**, *26*, 1219–1241. [[CrossRef](#)]
23. Li, J.; Qiu, Y.Y.; Li, C.W.; Zhang, Z. A Walker exponent corrected model for estimating fatigue life of metallic materials in loading with mean stress. *Mater. Werkst.* **2019**, *50*, 1106–1112. [[CrossRef](#)]
24. Kluger, K.; Lagoda, T. A new algorithm for estimating fatigue life under mean value of stress. *Fatigue Fract. Eng. Mater. Struct.* **2017**, *40*, 448–459. [[CrossRef](#)]
25. Liu, X.; Mao, K.; Wang, X.; Wang, X.; Wang, Y. A modified quality loss model of service life prediction for products via wear regularity. *Reliab. Eng. Syst. Saf.* **2020**, *204*, 107187. [[CrossRef](#)]
26. Korsunsky, V.; Dini, D.; Dunne, F.P.; Walsh, M.J. Comparative assessment of dissipated energy and other fatigue criteria. *Int. J. Fatigue* **2007**, *29*, 1990–1995. [[CrossRef](#)]
27. Ince, A.; Glinka, G. A modification of Morrow and Smith-Watson-Topper mean stress correction models. *Fatigue Fract. Eng. Mater. Struct.* **2011**, *34*, 854–867. [[CrossRef](#)]
28. Gao, Q.; Feng, J.Z.; Zheng, S.L. Optimization design of the key parameters of McPherson suspension systems using generalized multi-dimension adaptive learning particle swarm optimization. *Proc. Inst. Mech. Eng. Part D J. Automob. Eng.* **2019**, *233*, 3403–3423. [[CrossRef](#)]
29. Kamaya, M.; Kawakubo, M. Mean stress effect on fatigue strength of stainless steel. *Int. J. Fatigue* **2015**, *74*, 20–29. [[CrossRef](#)]
30. Wang, H.J.; Liu, X.T.; Chen, T.; Xu, S. Prediction and evaluation of fatigue life via modified energy method considering surface processing. *Int. J. Damage Mech.* **2022**, *31*, 426–443. [[CrossRef](#)]
31. Liang, W.; Conle, F.A.; Topper, T.H.; Walbridge, S. A review of effective-strain based and multi R-ratio crack propagation models and a comparison of simulated results using the two approaches. *Int. J. Fatigue* **2021**, *142*, 105920. [[CrossRef](#)]
32. Lukács, J.; Meilinger, Á.; Pósalaky, D. High cycle fatigue and fatigue crack propagation design curves for 5754-H22 and 6082-T6 aluminium alloys and their friction stir welded joints. *Weld. World* **2018**, *62*, 737–749. [[CrossRef](#)]
33. Fu, L.; Duan, H.; Li, H.; Lin, L.; Wang, Q.; Yao, J.; Luo, Y. Low-cycle fatigue behavior of 7075-T6 aluminum alloy at different strain amplitudes. *Mater. Express* **2020**, *10*, 942–947. [[CrossRef](#)]
34. Xu, X.; Xue, Q.; Ku, Z.; Li, H.; Hu, J. Improved fatigue damage accumulation analysis based on material memory property. *Int. J. Struct. Integr.* **2021**, *12*, 214–225. [[CrossRef](#)]
35. Narayanan, G. Probabilistic fatigue model for cast alloys of aero engine applications. *Int. J. Struct. Integr.* **2021**, *12*, 454–469. [[CrossRef](#)]

36. Wang, M.L.; Liu, X.T.; Wang, X.L.; Wang, Y.S. Probabilistic modeling of unified S-N curves for mechanical parts. *Int. J. Damage Mech.* **2018**, *27*, 979–999. [[CrossRef](#)]
37. Coffin, L.F. A study of the effects of cyclic thermal stresses on a ductile metal. *Trans. Am. Soc. Mech. Eng.* **1954**, *76*, 931–950. [[CrossRef](#)]
38. Morrow, J.D.; Socie, D.F. Review of contemporary approaches to fatigue damage analysis. *Risk Fail. Anal. Improv. Perform. Reliab.* **1980**, *24*, 141–194.
39. Dowling, N.E. *Mechanical Behavior of Materials*, 4th ed.; Prentice Hall: Hoboken, NJ, USA, 2012.
40. Lee, Y.L.; Pan, J.; Hathaway, R.; Barkey, M. *Fatigue Testing and Analysis: Theory and Practice*; Elsevier: Amsterdam, The Netherlands, 2005.
41. Budynas, R.G.; Nisbett, K.J. *Shigley's Mechanical Engineering Design ISE*, 11th ed.; McGraw-Hill: New York, NY, USA, 2019.
42. Mi, F. Investigation on Effects of the Mean Strain on Mechanical Behavior and Random Fatigue Life Prediction of an Aerospace Aluminum Alloy. Master's Thesis, Zhejiang University, Hangzhou, China, 2013.
43. *GB/T 15248-2008*; The Test Method for Axial Loading Constant-Amplitude Low Cycle Fatigue of Metallic Materials. Standards Press of China: Beijing, China, 2008.
44. Zhou, J.; Huang, H.Z.; Peng, Z.C. Fatigue life prediction of turbine blades based on a modified equivalent strain model. *J. Mech. Sci. Technol.* **2017**, *31*, 4203–4213. [[CrossRef](#)]

Disclaimer/Publisher's Note: The statements, opinions and data contained in all publications are solely those of the individual author(s) and contributor(s) and not of MDPI and/or the editor(s). MDPI and/or the editor(s) disclaim responsibility for any injury to people or property resulting from any ideas, methods, instructions or products referred to in the content.